A continuous parametric shape model

Asger Hobolth[1], Jan Pedersen[1] and Eva B. Vedel Jensen[1,2]
University of Aarhus

Summary

In the present paper we propose a flexible continuous parametric shape model for a star-shaped planar object. The model is based on a polar Fourier expansion of the normalized radius-vector function of the object. The expected phase amplitudes are modelled by a simple regression with parameters having simple geometric interpretations. The model is a generalization of first- and second-order Gaussian shape models and is called the generalized $p-$order model. In particular, non-Gaussian errors are allowed. The statistical analysis is straightforward, as demonstrated on a data set concerning shape discrimination of two cell populations.

Some key words: Cancer diagnostics; Featureless objects; Fourier descriptors; Radius-vector function; Shape; Star-shaped objects.

1   Introduction

Recently, shape modelling of featureless objects has attracted a lot of attention in the statistical literature. The Gaussian model with cyclic invariance properties, described by Grenander & Miller (1994), has played a predominant role.

One line of research has been concerned with the application of the Gaussian model as a prior model in Bayesian object recognition. Such an application has been discussed in Grenander & Miller (1994). The group around Håvard Rue has also contributed significantly to this research, cf. e.g. Rue & Syversveen (1998) and Rue & Hurn (1999). In Hansen et al. (2000) a similar

---

[1]Postal address: Laboratory for Computational Stochastics, Department of Mathematical Sciences, University of Aarhus, Ny Munkegade, DK-8000 Aarhus C, Denmark. Email addresses: asho@imf.au.dk, jan@imf.au.dk and eva@imf.au.dk.

[2]MaPhySto - Centre for Mathematical Physics and Stochastics, funded by the Danish National Research Foundation.

Bayesian analysis is performed where also the time aspect has been taken into account.

Another line of research has dealt with likelihood analysis of the Gaussian model. This approach is useful for describing rather than finding the objects. A very important contribution is the paper by Kent et al. (2000) where the model is used for modelling the standardized edge transformation vector, see also Kent et al. (1996). (The standardized edge transformation vector only contains shape information.) In particular, the eigendecomposition of the circulant covariance matrix is described. In the follow-up paper Hobolth et al. (1999) the corresponding theory is developed for the standardized vertex transformation vector. Likelihood analysis has also been considered in Hurn et al. (1999).

In Hobolth & Jensen (2000) a continuous approach is used, which may have a general appeal because the model and its parameters do not relate to a particular choice of the number of landmarks. Apart from that it appears natural to represent the boundary of an object continuously. The continuous counterpart of the standardized vertex transformation vector is the so-called normalized residual process, as introduced in Hobolth & Jensen (2000). Continuous models have also been mentioned in Hobolth et al. (1999) and Kent et al. (2000).

In the present paper we represent the shape of a random planar star-shaped object in terms of the normalized radius-vector function $R = (R(t))_{t \in [0,1]}$. A flexible continuous statistical model is proposed for R. Generally R need not be Gaussian. The main reason for choosing a specific representation of the object is that this allows us to analyse in detail the relationship between the model assumed for the normalized radius-vector function and the random geometry of the object.

Our approach rely on a polar Fourier expansion of the normalized radius-vector function

$$R(t) = 1 + 2\sqrt{c_1}\cos(2\pi(t - d_1)) + 2\sum_{s=2}^{\infty} \sqrt{C_s}\cos(2\pi s(t - D_s)), \quad t \in [0,1].$$

We show that the first phase amplitude c_1 and the first phase angle d_1 play a special role as parameters of asymmetry and discuss in detail how the remaining random phase amplitudes C_s and phase angles D_s influence the shape of the random object. The model proposed is called the generalized $p-$order model. Under this model the expected phase amplitudes $\lambda_s = E(C_s)$ satisfy the simple regression equation

$$\lambda_s^{-1} = \alpha + \beta(s^{2p} - 2^{2p}), \quad s \geq 2,$$

where $\alpha > 0$, $\beta > 0$ and $p > 1/2$. It will be shown that p determines the smoothness of the boundary of the object while the parameters α and β determine the 'global' and the 'local' shape, respectively.

The phase angles D_s are assumed to be uniformly distributed. There are, however, no restrictions on the distributions of the phase amplitudes C_s. Exponentially distributed amplitudes correspond to a Gaussian normalized radius-vector function. Generalized gamma distributed amplitudes offer a simple extension which allows for both heavier and lighter tails than the exponential ones.

In Section 2, the geometry of the radius-vector function is analysed in detail. This analysis is the basis for the construction of the generalized p-order model in Section 3. Its statistical inference is discussed in Section 4. The model is applied in Section 5 to a data set of normal mantle cell nuclei and cell nuclei from a mantle lymphoma. It turns out that the cell nuclei from the mantle lymphoma are more 'irregular' than the normals cells (significantly different β-values in the two groups). Shape discrimination of these two cell nuclei types was our original motivation for studying the continuous shape model. Section 6 contains some ideas for future research.

2 The geometry of the radius-vector function

Let K be a compact subset of $\mathbf{R}^2$. Let us suppose that K is star-shaped with respect to $z \in K$, i.e. the intersection between every line through z and K is a line segment. We will describe K in terms of its radius-vector function $(r_K(t; z))_{t \in [0,1]}$ with respect to z, where

$$r_K(t; z) = \max\{r : z + r(\cos 2\pi t, \sin 2\pi t) \in K\}, \quad t \in [0, 1].$$

The value $r_K(t; z)$ is the distance from z to the boundary of K along the ray, starting at z and with angle $2\pi t$ relative to a fixed axis. Because K is star-shaped we can reconstruct K from $r_K(\cdot; z)$.

The radius-vector function is well-known in the shape literature, cf. e.g. Stoyan & Stoyan (1994, p. 63), Lestrel (1997), Loncaric (1998) and references therein. It is also an important quantity in local stereology and geometric tomography, cf. Jensen (1998, Chapters 4 and 5) and Gardner (1995, Section 0.7). The radius-vector function is in geometric tomography called the radial function.

Using Hobolth & Jensen (2000, Proposition 1) it can be seen that the derivative (if it exists) of the radius-vector function contains interesting geometric information

$$r_K'(t; z) = 2\pi \cot(\varphi_K(t; z) - 2\pi t) r_K(t; z),$$

where $\varphi_K(t; z)$ is the angle that the tangent of the boundary point of K at position t makes with a fixed axis. The tangent-angle function $\varphi_K(\cdot; z)$ is therefore obtainable from the radius-vector function. The reverse statement

is also true, but then the radius-vector function is only determined up to a multiplicative constant. The second derivative of $r_K(\cdot; z)$ involves the local curvature of K.

The area and boundary length of K can be expressed in terms of the radius-vector function

$$
\begin{aligned}
A(K) &= \pi \int_0^1 r_K(t; z)^2 dt \\
B(K) &= 2\pi \int_0^1 \{r_K(t; z)^2 + (2\pi)^{-2} r'_K(t; z)^2\}^{1/2} dt \\
&= 2\pi \int_0^1 r_K(t; z)/|\sin(\varphi_K(t; z) - 2\pi t)| dt.
\end{aligned}
$$

The formula for area holds without further assumptions, while the formula for boundary length holds under mild assumptions about K, including that the boundary of K is smooth, cf. Stoyan & Stoyan (1994, p. 64) and Jensen (1998, Proposition 5.4). It is also possible to express the total curvature of K in terms of $r_K(\cdot; z)$.

The definition of the radius-vector function can be extended to not-necessarily star-shaped sets K, cf. Gardner et al. (1995). The extended function is the radius-vector function of a star-shaped set associated with K, called the directed chordal symmetrical.

The radius-vector function is invariant under translation and rotation. To be more specific, let $z_0 \in \mathbf{R}^2$ and

$$
A = \begin{pmatrix} \cos 2\pi t_0 & -\sin 2\pi t_0 \\ \sin 2\pi t_0 & \cos 2\pi t_0 \end{pmatrix}, \quad t_0 \in [0, 1].
$$

Then,

$$
r_{AK+z_0}(t; Az + z_0) = r_K((t - t_0) \bmod 1; z), \quad t \in [0, 1].
$$

A scaling transformation yields

$$
r_{\alpha K}(t; \alpha z) = \alpha r_K(t; z), \quad t \in [0, 1], \quad \alpha > 0.
$$

The shape of K is thus, up to shifts in t, represented by the normalized radius-vector function

$$
\widetilde{r}_K(t; z) = \frac{r_K(t; z)}{\int_0^1 r_K(u; z) du}, \quad t \in [0, 1].
$$

Note that the normalized radius-vector function is a continuous analogue of a standardized vertex transformation vector, cf. Hobolth et al. (1999). Below we will simply write $r(\cdot)$ for $\widetilde{r}_K(\cdot; z)$ in cases where it will cause no confusion.

A more detailed description of the shape of K can be obtained from a Fourier series expansion of the normalized radius-vector function r, cf. e.g. Stoyan & Stoyan (1994, p. 80-88) and Lestrel (1997),

$$r(t) = 1 + \sqrt{2} \sum_{s=1}^{\infty} a_s \cos(2\pi st) + \sqrt{2} \sum_{s=1}^{\infty} b_s \sin(2\pi st), \quad t \in [0, 1],$$

where the Fourier coefficients are

$$a_s = \sqrt{2} \int_0^1 r(t) \cos(2\pi st) dt, \quad b_s = \sqrt{2} \int_0^1 r(t) \sin(2\pi st) dt, \quad s \geq 1. \quad (2.1)$$

The Fourier coefficient at phase 0 is 1 because of the normalization of the radius-vector function. Letting

$$a_s = \sqrt{2c_s} \cos(2\pi s d_s), \quad b_s = \sqrt{2c_s} \sin(2\pi s d_s), \quad s \geq 1,$$

we obtain the polar form

$$r(t) = 1 + 2 \sum_{s=1}^{\infty} \sqrt{c_s} \cos(2\pi s(t - d_s)), \quad t \in [0, 1], \quad (2.2)$$

where $c_s = (a_s^2 + b_s^2)/2 \geq 0$ and $d_s \in [0, \frac{1}{s}[, s \geq 1$. (If $a_s = b_s = 0$, let $d_s = 0$.) The coefficient c_s is called the sth phase amplitude and d_s the sth phase angle. It is immediate from (2.2) that the c_ss are invariant under shifts in t.
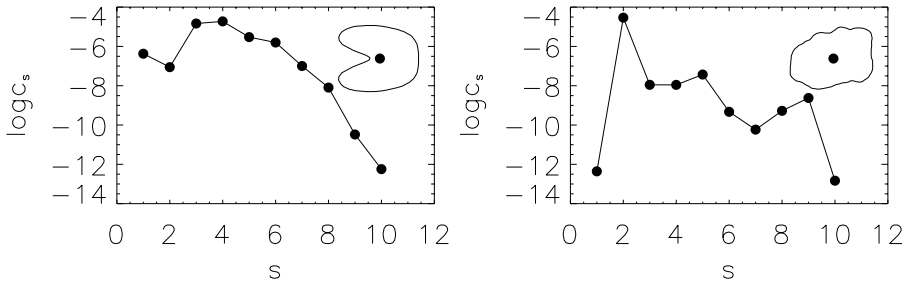
Figure 1: The values of the phase amplitudes c_s are shown as a function of s for an asymmetric object (left) and a fairly symmetric object (right).

Writing $z = (z_1, z_2)$, the boundary of K can be represented as

$$(f_1(t), f_2(t)) = (z_1, z_2) + qr(t) (\cos(2\pi t), \sin(2\pi t)), \quad t \in [0, 1],$$

where q is the integral of the radius-vector function. Combining this with (2.1) it follows that

$$(a_1, b_1) = \frac{\sqrt{2}}{q} \left(\int_0^1 [f_1(t) - z_1] dt, \int_0^1 [f_2(t) - z_2] dt \right).$$

Thus, if K is symmetric (with respect to z) then $a_1 = b_1 = c_1 = 0$. Conversely, a high value of c_1 indicates a high degree of asymmetry relative to z, cf. Figure 1. The left object in Figure 1 is an example of an object which is symmetric around the $x-$axis, but rather asymmetric around the $y-$axis. If the angle $2\pi t$ is measured relative to the $x-$axis this means that a_1 is rather large while $b_1 = 0$. In the Appendix we show that the Fourier coefficients a_1 and b_1 can also be expressed as integrals on the interior of K.

To analyse the geometry of the higher order phase amplitudes let us consider an object for which all but the sth phase amplitude are zero such that

$$r(t) = 1 + 2\sqrt{c_s} \cos(2\pi s(t - d_s)). \tag{2.3}$$

For such an object we have that z is the centre of gravity, cf. the Appendix. Moreover, $r(t)$ possesses an s-fold symmetry,

$$r(t) = r(t + \frac{1}{s}) = \cdots = r(t + \frac{s-1}{s}), \quad t \in [0, \frac{1}{s}[.$$

The 2-fold symmetry is the usual type of symmetry. In Figure 2 we have plotted objects with radius-vector function of the form (2.3), corresponding to different values of s, $d_s = 0$ and varying values of c_s. In Figure 3 we have
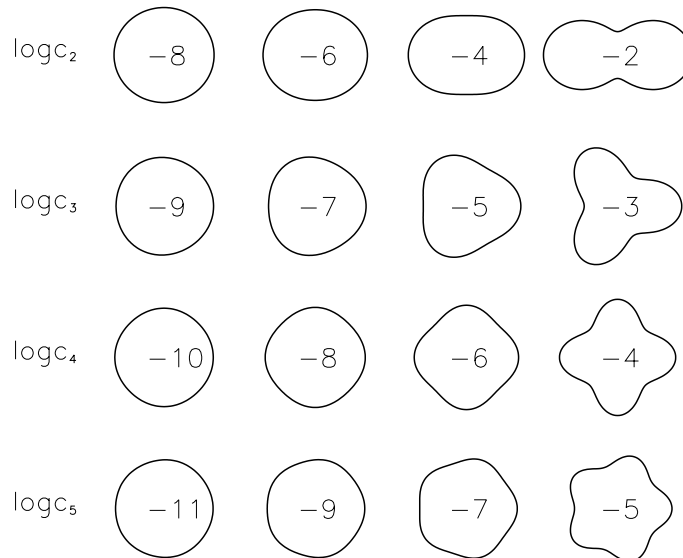
Figure 2: Objects with radius-vector function of the form (2.3) with $d_s = 0$. In each row the value of s is constant ($s = 2, 3, 4, 5$). The value of $\log c_s$ is indicated in the interior of the object.

illustrated how the $s-$fold symmetric objects contribute for small s to the 'global' shape of a given object K and for large s to the 'local' shape.
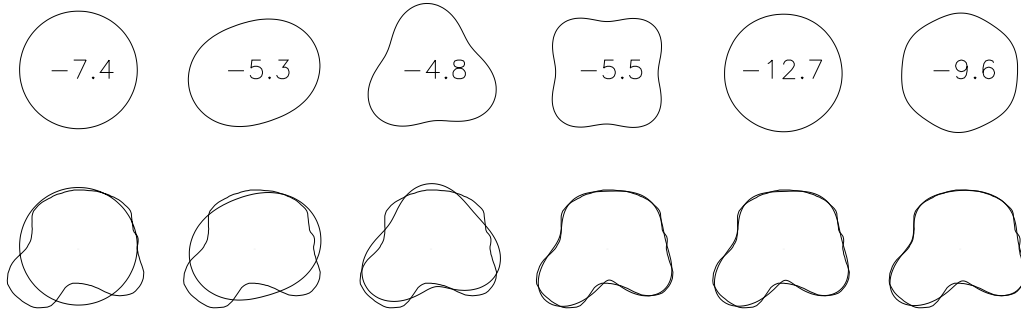
Figure 3: The upper row shows the objects of the form (2.3) for $s = 1, \ldots, 6$ (left to right) associated with the object K shown in the lower row. The values of $\log c_s$ are indicated in their interior. In the lower row, the reconstruction of K from the first s Fourier coefficients is also shown.

To sum up, we can interpret $c_s, s \geq 1$, as shape parameters. For $s = 1$, c_s is an asymmetry parameter. For $s \geq 2$ small, c_s determines the 'global' shape of K while for s large c_s affects the 'roughness' of the boundary of K. Up to a shift in t, d_s, $s \geq 1$, are also shape parameters. For $s \geq 2$, they determine the relative orientation of the $s-$fold symmetric objects associated with K.

In Zahn & Roskies (1972) the geometric interpretation of a Fourier expansion of the tangent-angle function is studied in a similar way.

Let us conclude this section by discussing how z can be chosen. In some applications z is 'given by nature'. An important example comes from local stereology where K is actually a planar section through a biological cell, passing through the nucleus or nucleolus of the cell, cf. Jensen (1998, Chapter 7). In other cases z is defined from K, typically as the centre of mass, cf. Loncaric (1998) and Hobolth et al. (1999). In the latter paper it is used that with z equal to the centre of gravity the first phase amplitude of $r_K(\cdot; z)$ is approximately zero when K is a small deformation of a circle. In the Appendix it is shown that the centre of mass of K can in fact be characterized by the property that the first phase amplitude of $r_K(\cdot; z)^3$ is zero.

3 The generalized p-order model

We will now consider a random planar object K with normalized radius-vector function $(R(t))_{t \in [0,1]}$. Below we introduce the parametric statistical model to be used for R.

The starting point is the polar expansion (2.2) of the normalized radius-vector function. As argued in the previous section the first phase angle d_1 and phase amplitude c_1 play a special role as asymmetry parameters. We shall

7

treat c_1 and d_1 as non-random nuisance parameters. The expansion of the normalized radius-vector function in polar form therefore becomes

$$R(t) = 1 + 2\sqrt{c_1}\cos(2\pi(t - d_1)) + 2\sum_{s=2}^{\infty}\sqrt{C_s}\cos(2\pi s(t - D_s)), \ t \in [0, 1]. \quad (3.1)$$

The remaining amplitudes C_s and angles D_s, $s \geq 2$, will be modelled by distributions on $\mathbf{R}_+$ and $[0, 1/s]$, respectively.

The expansion (3.1) makes it possible to construct a variety of shape models. A *generalized $p-order$ model* is a parametric model which satisfies that

$$C_s \sim \lambda_s Z_s, \quad D_s \sim U[0, 1/s], \quad s \geq 2, \quad (3.2)$$

where the error variables Z_s have mean 1 and $U[0, 1/s]$ is the uniform distribution on the indicated interval. Furthermore, $C_s, D_s, s \geq 2$, are all independent and the expected phase amplitudes $\lambda_s = E(C_s)$ decrease as

$$\lambda_s^{-1} = \alpha_0 + \beta s^{2p}, \quad s \geq 2.$$

The parameters satisfy $\alpha_0 > -\beta 2^{2p}$ and $\beta > 0$ such that $\lambda_s > 0$ for all $s \geq 2$. We further assume $p > 1/2$, which implies that R has finite variance, as will be discussed below.

In order to facilitate a geometric interpretation of the regression parameters we use the reparametrization

$$\lambda_s^{-1} = \alpha + \beta(s^{2p} - 2^{2p}), \quad s \geq 2, \quad (3.3)$$

where $\alpha > 0, \beta > 0, p > 1/2$. The parameter α determines the 'global' shape of the object. If α is high objects of circular shape are expected while a low value corresponds to an elongated or, in the extreme, a 'peanut-shell' shape. The reason is that under (3.3), α determines the expected phase amplitudes $\lambda_s = E(C_s)$ for small s and C_s governs the global shape for small s, cf. Section 2. As discussed below p determines the smoothness of the boundary of K. For fixed p the parameter β determines the 'local' shape of the object since it controls the behaviour of λ_s when s is high. Precisely, as $s \to \infty$, we have that $(\log s, \log \lambda_s^{-1})$ behaves as a line with slope $2p$ and intercept $\log \beta$. For small values of β rather irregular objects are expected while high values yield regular objects.

The random phase angles D_s determine the relative orientation of the $s-$fold symmetric objects associated with K, cf. Section 2. The uniform distribution on the angles implies that these objects do not have a 'preferred orientation'. A generalized $p-order$ model is therefore expected to be appropriate for describing a population of objects which does not have a predominant non-circular shape. The shape variability of K is influenced by the variation of the error variables Z_s.

8

In Figure 4 simulations from the model (3.1)-(3.3) with exponentially distributed error variables, $p = 2$ and $c_1 = 0$ are shown. The values of α and β are typical for the objects studied in the data section. It is seen that in the corner corresponding to high values of α and β the simulated objects are smooth and 'circle'-like, while in the opposite corner the simulated objects are irregular.
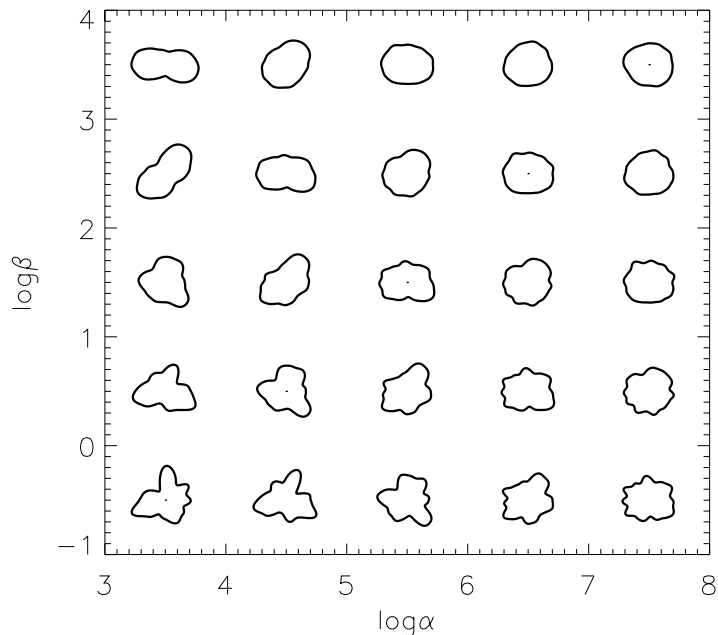
Figure 4: Simulated objects under the second-order model with $c_1 = 0$, exponentially distributed error variables and the indicated values of α and β.

To study the distribution of the radius-vector function let

$$R_1(t) = 2 \sum_{s=2}^{\infty} \sqrt{C_s} \cos(2\pi s(t - D_s)), \quad t \in [0, 1],$$

contain all the random Fourier terms of $R(t)$. Using (3.2) and independence of the phase angles and amplitudes it follows that R_1 is a stationary process with covariance function

$$\sigma(t) = \mathrm{cov}(R_1(t), R_1(0)) = 2 \sum_{s=2}^{\infty} \lambda_s \cos(2\pi st), \quad t \in [0, 1]. \tag{3.4}$$

The process R_1 has zero Fourier coefficients at phases 0 and 1. Similar constraints were used by Hobolth et al. (1999) and Kent et al. (2000) in a discrete time model. Properties such as continuity and differentiability of R_1

9

(and hence also of R) are determined by the parameter p as follows from Cramér & Leadbetter (1967, Section 4.2 and 4.3).

Equation (3.4) gives the relation between the expected amplitudes and the covariance function. As an alternative to parametric specification of the λ_ss as in (3.3) one may suggest a simple parametric form of the covariance function σ, cf. e.g. Rue & Syversveen (1998). Since the amplitudes relate to the random geometry of the object we believe it is more natural to specify directly a parametric model for the expected amplitudes. Furthermore, the constraints on R_1 are easier to handle and interpret in the spectral domain.

In the shape literature a random object is often modelled by a multivariate normal distribution with a circulant covariance matrix or by a stationary Gaussian process in continuous time, cf. Grenander & Miller (1994), Hobolth et al. (1999), Rue & Hurn (1999), Hobolth & Jensen (2000), Kent et al. (2000). We now show that a Gaussian model is obtained by letting the error variables Z_s be exponentially distributed. This model will therefore be called the normal $p-$order model. Using (2.2) and (3.2) it follows that if Z_s is exponentially distributed then

$$R_1(t) = \sqrt{2} \sum_{s=2}^{\infty} A_s \cos(2\pi st) + \sqrt{2} \sum_{s=2}^{\infty} B_s \sin(2\pi st), \quad t \in [0, 1],$$

where $A_s, B_s, s \geq 2$, are all mutually independent and $A_s \sim B_s \sim N(0, \lambda_s)$. This representation shows that R_1 is a stationary Gaussian process. By (3.3) and Rogers & Williams (1994, Theorem I.25.10), it follows that for the normal $p-$order model the sample paths of R_1, and hence also of R, are k times continuously differentiable where k is the integer satisfying $p \in]k-1/2, k+1/2]$. In particular, if p is an integer then $p = k$. In the normal first-order model, the sample paths of R are continuous while in the normal second-order model the sample paths are continuously differentiable.

The first- and second-order normal models have been studied in the literature (most often without the constraint $\lambda_0 = \lambda_1 = 0$). In particular, these models appear as limits of discrete time first- and second-order Markov models, cf. e.g. Grenander (1993, p. 476 and 484).

4   Some remarks on statistical inference

Maximum likelihood estimation of the parameters of the normal $p-$order model, based on a continuously observed normalized radius-vector function, has been discussed in an unpublished research report by two of us (A. Hobolth and J. Pedersen) from Laboratory for Computational Stochastics, University of Aarhus, 1999. (In this report, we also suggest the regression equation (3.3), which was later used in Hobolth et al. (1999).) For the first- and second-order

normal models it is shown that with continuous observations β is determined with certainty from observable quantities. Thus, only α has to be estimated and a closed-form equation for the maximum likelihood estimate of α is given in the research report.

Although the likelihood-based estimates have several good properties in theory, they may perform poorly in practice. Thus, as expected from the interpretation of the parameter β as a local shape parameter, β is determined from differences between observations very close together at the boundary of the object under study. If only a digitized version of the object is available such differences cannot be determined accurately.

To avoid this obstacle one can use a so-called low-pass filter, cf. e.g. Bloomfield (1976). The idea is to determine the parameter estimates from the low frequency Fourier coefficients only which are robust against digitization effects. For the normal $p-$order model, the analysis is particularly simple. Recall that in this case the phase angles D_s are uniform in $[0, 1/s]$ and the phase amplitudes C_s are exponentially distributed with mean λ_s. Note in particular that the distribution of the phase angles does not depend on unknown parameters. Using the first S phase amplitudes the likelihood function becomes

$$L(\lambda_s; c_s) = \prod_{s=2}^{S} \lambda_s^{-1} e^{-\lambda_s^{-1} c_s}. \tag{4.1}$$

Defining the expected amplitudes by (3.3) the maximum likelihood estimates for (α, β, p) can be found by standard numerical methods. A likelihood function of the same form has been considered in Hobolth et al. (1999) and Kent et al. (2000).

If the normalized radius-vector function is only known at the data points $t = 0/n, 1/n, \ldots, (n-1)/n$, the phase amplitudes $c_s = (a_s^2 + b_s^2)/2$ can be approximated by using discretized versions of the integrals (2.1). The specific value of n is not important, just as long as it is reasonably high. That is, different values of n give approximately the same value of c_s.

5 Data analysis

The data set consists of 50 normal mantle cell nuclei and 50 cell nuclei from a mantle lymphoma (tumour in the mantle zone of a lymph node), cf. Figure 5. The nuclei from each of the groups were sampled from a microscopic section among those with sectioned boundary in focus. The normalized radius-vector function $r(t)$ with respect to the centre of mass was for each nucleus determined at $t = 0, 1/n, \ldots, (n-1)/n$. Unless otherwise stated we used $n = 100$. The nuclei are rather homogeneous in size (about $15\mu m$ in diameter), so the normalization factor was almost the same for all the nuclei.

11
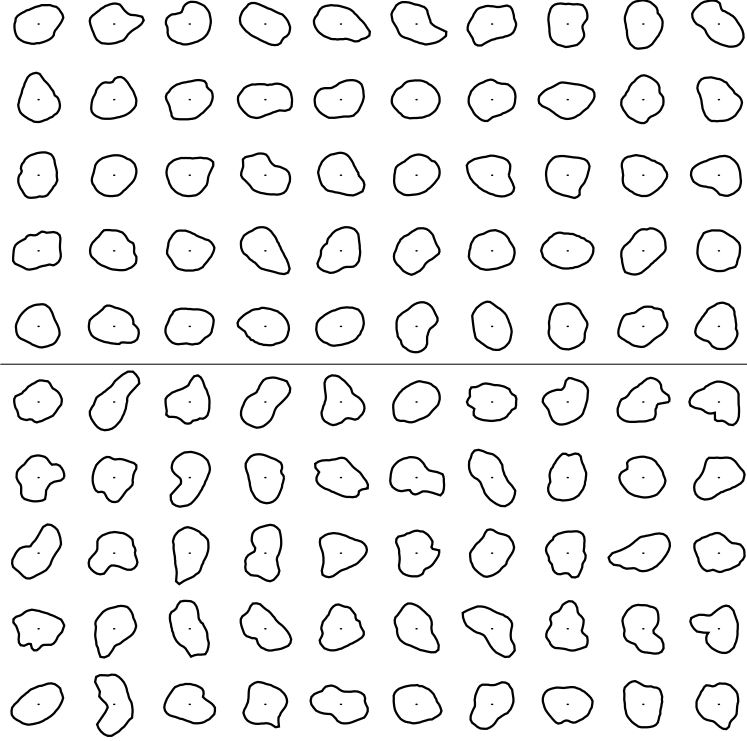
Figure 5: The 50 normal mantle cell nuclei (upper panel) and the 50 cell nuclei from a mantle lymphoma (lower panel).

5.1 Analysing each nuclear profile individually

First, each nuclear profile was analysed individually using the likelihood function (4.1). The choice of cut-off value S is important. If S is too small we are not using important shape information; if on the other hand S is too large the results will be influenced by digitization effects, see also Figure 3. Unless otherwise stated we used $S = 15$.

For each object we found the estimates of (α, β, p). In both samples the estimates of p were close to 2 for all nuclei. For the normal sample the average was 2.07 with a standard deviation of 0.21 while for the lymphoma sample the average was 2.02 and the standard deviation 0.28. Therefore we fixed $p = 2$ and considered the normal second-order model only.

The estimates of (α, β) under the second-order model are shown for each nucleus in Figure 6 and summarized in Table 1. The estimates of the local shape parameter β are on average lowest in the lymphoma sample. This was to be expected from the geometric interpretation of β given in Section 3. A t-test for identical βs, based on the distribution of $\log \hat{\beta}$, shows a significant difference between the two samples (p-value less than 0.05%). On average the estimates of the global shape parameter α are also lowest in the lymphoma sample, but
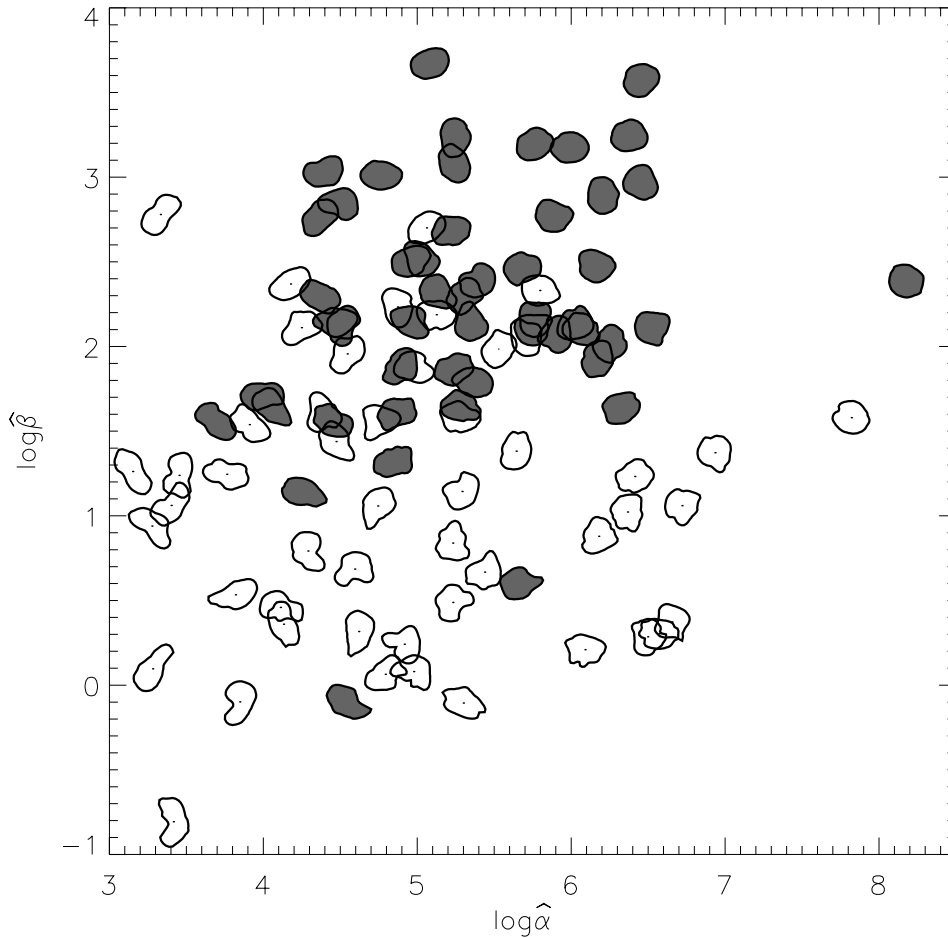
Figure 6: The estimates of (α, β) under the normal second-order model. The hatched nuclei are from the normal mantle cells while the white nuclei are from cells in the mantle lymphoma.

	$\log \hat{\alpha}$		$\log \hat{\beta}$		
	av.	s.d.	av.	s.d.	corr.
normal	5.35	0.84	2.26	0.72	0.27
lymphoma	4.94	1.11	1.09	0.81	0.03

Table 1: The average, standard deviation and correlation of $(\log \hat{\alpha}, \log \hat{\beta})$ for each sample.

the difference is not as significant (p-value close to 5%). Furthermore we see that the estimates of α from the lymphoma sample vary over a somewhat

larger range than the estimates from the normal sample.

We also investigated how the choice of cut-off value S influences the analysis. Since the estimate of α is determined by the first few amplitudes the estimate of this parameter only changes slightly when S is larger than 8, say. From Figure 7 it is seen that the estimate of β does change with S, but the changes are rather small.
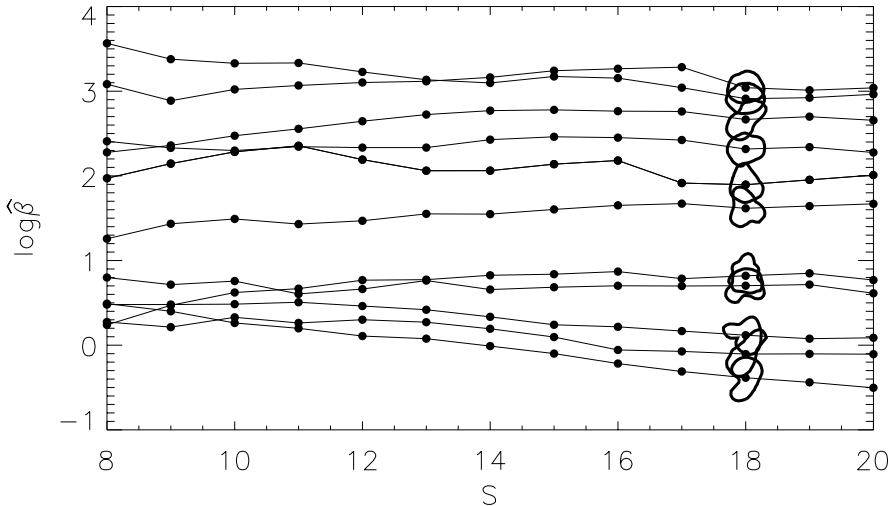
Figure 7: The estimates of β as a function of S for the 11 nuclei shown.

The number of data points n should be high compared to S, but otherwise the specific choice is less important. In Figure 8 we see that for $S = 15$ the estimates are stable, and the analysis is robust to the specific choice of $n \geq 50$.

5.2 Analysing the profiles under an iid-assumption

We now investigate whether the profiles within each of the groups can be regarded as independent and identically distributed realizations from a normal $p-$order model. Let the indices (i, j) denote the jth nucleus ($j = 1, \ldots, N = 50$) in the normal sample ($i = 1$) or the lymphoma sample ($i = 2$) and let c_{sij} be the corresponding phase amplitudes of the normalized radius-vector function. If we let $\mathrm{Exp}(\lambda)$ be the notation used for the exponential distribution with mean λ, we then want to investigate whether

$$C_{sij} \sim \mathrm{Exp}(\lambda_{si}), \quad j = 1, \ldots, N, \tag{5.1}$$

for each $s = 2, \ldots, S$ and $i = 1, 2$.

14
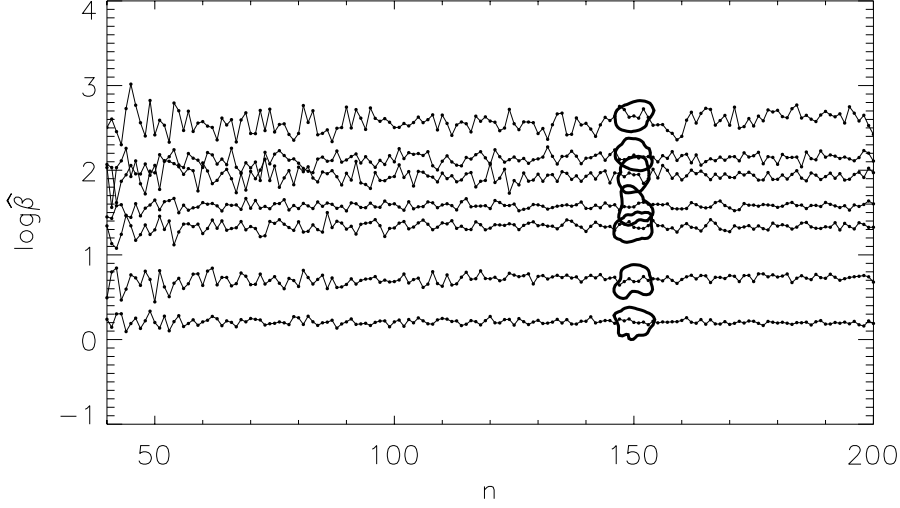
Figure 8: The estimates of β as a function of n for the 7 nuclei shown.

We will examine (5.1) by considering the more general model

$$C_{sij} \sim \Gamma(\gamma_{si}, \rho_{si}, \delta_{si}), \quad j = 1, \ldots, N,$$

where $\Gamma(\gamma, \rho, \delta)$ is the notation used for the generalized gamma distribution with density

$$f(y) = \frac{\delta y^{\delta\gamma-1}}{\Gamma(\gamma)\rho^{\delta\gamma}} \exp\{-(\frac{y}{\rho})^\delta\}, \quad y > 0.$$

Here, $\gamma, \delta > 0$ are shape parameters while $\rho > 0$ is a scale parameter. The ordinary gamma distribution is obtained for $\delta = 1$, the Weibull distribution for $\gamma = 1$, while the exponential distribution corresponds to $\delta = \gamma = 1$.

The class of generalized gamma distributions is in fact rather flexible. When $\delta < 1$ (> 1) the tails are heavier (lighter) than the exponential tails. When $\delta\gamma \leq 1$ the density $f(y)$ is strictly decreasing in y. Moreover $\lim_{y\to 0} f(y)$ exists and is finite if and only if $\delta\gamma \geq 1$. When $\delta\gamma > 1$ the density has a mode.

Plots of the empirical survival functions of c_{sij} for fixed s and i showed that the distributions of the phase amplitudes had somewhat heavier tails than expected under (5.1) (the estimated values of δ were less than 1). In each sample the tendency was only significant for a few high values of s. Thus it seems reasonable to consider exponentially distributed error variables, at least for low frequencies. The same conclusion was obtained by testing (5.1) by Bartlett tests.

Assuming that the phase amplitudes c_{sij} are $\text{Exp}(\lambda_{si})$-distributed, the next

15

step in the analysis is to fit a p-order model within each group,

$$\lambda_{si}^{-1} = \alpha_i + \beta_i \left(s^{2p_i} - 2^{2p_i}\right), \quad s = 2, \ldots, S, \quad i = 1, 2. \tag{5.2}$$

The likelihood function is given by

$$L(\lambda_{si}; c_{sij}) = \prod_{j=1}^{N}\prod_{s=2}^{S} \lambda_{si}^{-1} \exp(-\lambda_{si}^{-1}c_{sij}) = \{\prod_{s=2}^{S} \lambda_{si}^{-1} \exp(-\lambda_{si}^{-1}\bar{c}_{si.})\}^N,$$

where $\bar{c}_{si.} = N^{-1}\sum_{j=1}^{N} c_{sij}$ is the average of the amplitudes within the ith group at phase s and λ_{si} is given by (5.2). As expected the estimated value of p is close to 2 in both samples (2.0 in the normal and 1.8 in the lymphoma sample), and again we consider the second-order model. The estimated regression lines are shown in Figure 9 and in Table 2 the estimates and approximate standard errors and correlation coefficients based on the observed information are summarized.
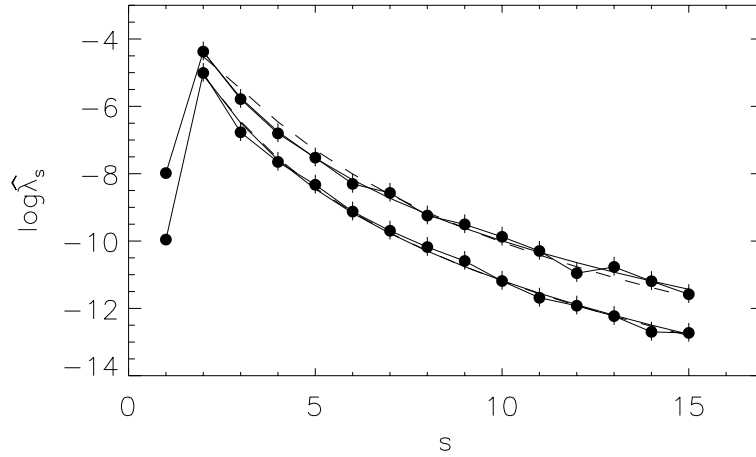
Figure 9: The estimated regression $\hat{\lambda}_s = [\hat{\alpha} + \hat{\beta}(s^{2\hat{p}} - 2^{2\hat{p}})]^{-1}$ in the normal p-order model (solid) and the estimated regression under the normal second-order model (dashed) is shown together with the average phase amplitudes as a function of s for the normal sample (lower curve) and the lymphoma sample (upper curve). The vertical lines are the 95% confidence limits.

As in the previous subsection we observe a significant difference between the two samples in the value of β. The difference in α is not as significant.

5.3   Simulations from the normal second-order model

In the normal second-order model truncated at $S = 15$ we have

$$C_s \sim \text{Exp}(\lambda_s), \quad s = 2, \ldots, 15, \quad \text{independent,}$$

	log $\hat{\alpha}$			log $\hat{\beta}$			
	est.	conf.int.	s.e.	est.	conf.int.	s.e.	corr
normal	5.08	4.81-5.35	0.14	1.97	1.89-2.05	0.04	-0.10
lymphoma	4.52	4.27-4.77	0.13	0.82	0.74-0.90	0.04	-0.13

Table 2: The estimates and approximate confidence intervals, standard errors and correlation of $(\log \hat{\alpha}, \log \hat{\beta})$.

with

$$\lambda_s^{-1} = \alpha + \beta(s^4 - 2^4). \tag{5.3}$$

In order to investigate the model more closely we made the following simulation study. For each sample we calculated λ_s according to (5.3) with (α, β) replaced by the average estimated value from Table 1 and simulated $C_s \sim \text{Exp}(\lambda_s), s = 2, \ldots, 15$. From the values of C_s we calculated the maximum likelihood estimates of α and β. This procedure was repeated 500 times for each of the samples and the results are shown in Figure 10 and summarized in Table 3.

	log $\hat{\alpha}$		log $\hat{\beta}$		
	av.	s.d.	av.	s.d.	corr.
normal	5.36	1.01	2.28	0.30	-0.14
lymphoma	4.89	0.95	1.10	0.30	0.03

Table 3: The average, standard deviation and correlation of $(\log \hat{\alpha}, \log \hat{\beta})$ for each sample.

When we compare Figures 6 and 10 it is seen that the variation in $\log \hat{\alpha}$ is almost the same for the observed and simulated data for both groups. The variation range of $\log \hat{\beta}$ is smaller in the simulation study than in the samples. One explanation is that the local shape variability in the data is somewhat higher than predicted from the normal model, i.e. the assumption that the error variables are exponential is not appropriate at high phases. Another reason might be that a well located 'blob' results in many high phase amplitudes.

6 Perspectives

The generalized p-order model is expected to be useful for describing a population which does not have a predominant non-circular shape. Let us stress, though, that the Fourier expansion (3.1) of the normalized radius-vector function makes it possible to construct a variety of shape models. If, for instance,
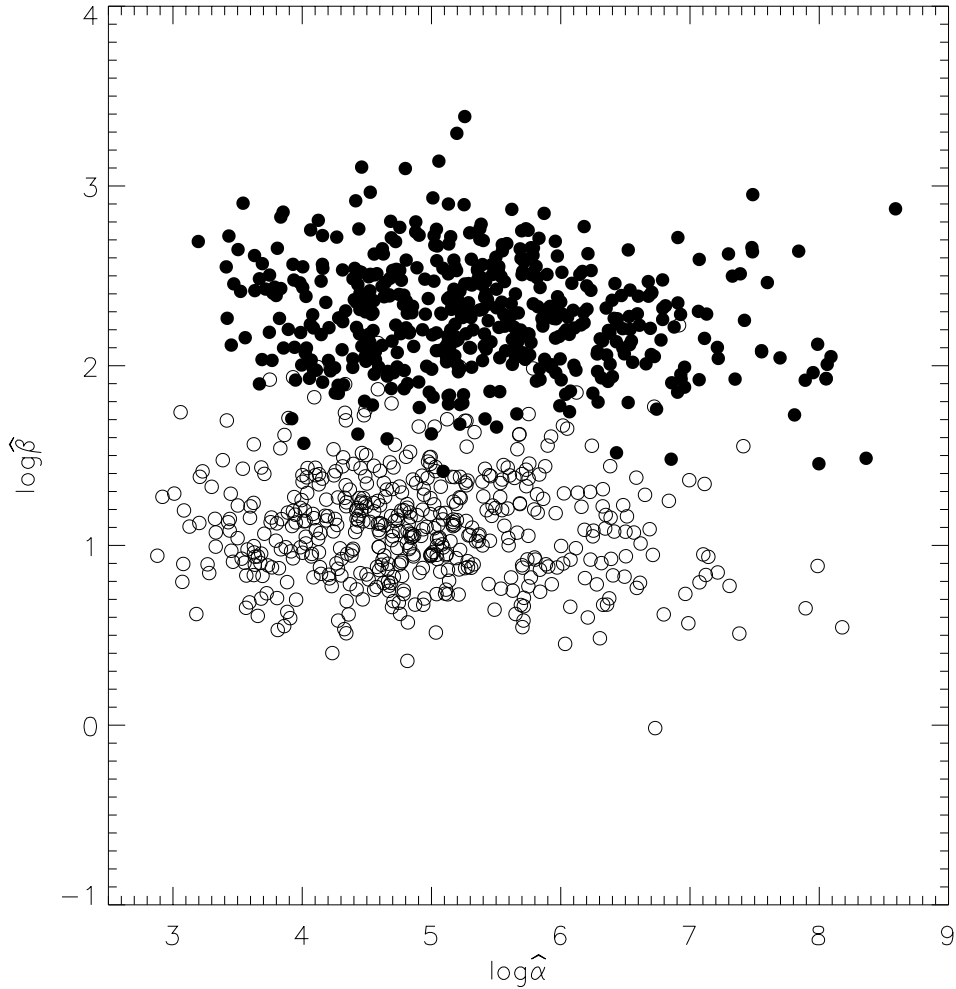
Figure 10: Simulated distribution of $(\hat{\alpha}, \hat{\beta})$ under the normal second-order model is shown for the normal sample (•) and the lymphoma sample (◦).

one considers a population with a dominant triangular shape, it would be natural to use a model where on average C_3 is the highest amplitude. A more challenging task is to model objects with a dominant elliptical shape. An ellipse has vanishing amplitudes at odd phases and decreasing amplitudes at even phases. Thus, to model elliptical shape one should probably let the odd and even amplitudes decrease at different rates. Moreover, the even phase angles should have approximately the same values. Elliptical models were studied by Hobolth & Jensen (2000). We leave a concrete model as a topic for future research.

Acknowledgements

Appendix

Characterization of asymmetry and centre of mass

Let $x = (x_1, x_2)$ denote a generic point in $\mathbf{R}^2$ and let $||x|| = (x_1^2 + x_2^2)^{\frac{1}{2}}$.

Proposition *Let $z = (z_1, z_2)$ be an interior point of a compact subset K of $\mathbf{R}^2$. Let K be star-shaped with respect to z and let the radius-vector function $r_K(t; z)$ be continuously differentiable in t.*

(i) *We have*

$$\int_K \frac{x_1 - z_1}{||x - z||^2} dx_1 dx_2 = 2\pi \int_0^1 r_K(t; z) \cos(2\pi t) dt \qquad (A.1)$$

$$\int_K \frac{x_2 - z_2}{||x - z||^2} dx_1 dx_2 = 2\pi \int_0^1 r_K(t; z) \sin(2\pi t) dt. \qquad (A.2)$$

(ii) *If z is the centre of mass of K then*

$$\int_0^1 r_K(t; z)^3 \cos(2\pi t) dt = \int_0^1 r_K(t; z)^3 \sin(2\pi t) dt = 0. \qquad (A.3)$$

   Conversely, if z is such that (A.3) is satisfied then z is the centre of mass of K.

(iii) *Let $r_K(t; z) = 1 + 2\sqrt{c_s} \cos\left(2\pi s(t - d_s)\right)$, where $s \geq 2, 0 \leq c_s \leq 1/4$ and $d_s \in [0, \frac{1}{s}[$. Then z is the centre of mass of K.*

Proof. Let $F : [0, 1]^2 \rightarrow \mathbf{R}^2$ be defined by

$$F(v, t) = (z_1, z_2) + v r_K(t; z)(\cos(2\pi t), \sin(2\pi t)) .$$

Then F is onto K and $\left|\det\left(F'(v, t)\right)\right| = 2\pi v r_K(t; z)^2$. In order to prove (A.1) note that if $x = (x_1, x_2) \in K$ is such that $x = F(v, t)$ then

$$\frac{x_1 - z_1}{||x - z||^2} = \frac{\cos(2\pi t)}{v r_K(t; z)},$$

19

and from the transformation theorem we get

$$\int_K \frac{x_1 - z_1}{||x - z||^2} dx_1 dx_2 = 2\pi \int_0^1 r_K(t; z) \cos(2\pi t) dt.$$

The result (A.2) is proved similarly.

The same kind of arguments show that

$$\left(\int_K (x_1 - z_1) dx_1 dx_2, \int_K (x_2 - z_2) dx_1 dx_2 \right) \tag{A.4}$$
$$= \frac{2\pi}{3} \left(\int_0^1 r_K(t; z)^3 \cos(2\pi t) dt, \int_0^1 r_K(t; z)^3 \sin(2\pi t) dt \right).$$

The left-hand side is zero if and only if z is the centre of mass of K. Therefore (ii) is an immediate consequence of (A.4).

To prove (iii) one has to show that $r_K(t; z) = 1 + 2\sqrt{c_s} \cos(2\pi s(t - d_s))$ satisfies the condition (A.3). This follows from elementary calculations, and is left to the reader.

References

Bloomfield, P. (1976). *Fourier Analysis of Time Series: an Introduction*. New York: Wiley.

Cramér, H. & Leadbetter, M.R. (1967). *Stationary and Related Stochastic Processes*. New York: Wiley.

Gardner, R. (1995). *Geometric Tomography*. New York: Cambridge University Press.

Grenander, U. (1993). *General Pattern Theory*. Oxford: Oxford University Press.

Grenander, U. & Miller, M.I. (1994). Representations of knowledge in complex systems (with discussion). *J. R. Statist. Soc.* B **56**, 549-603.

Hansen, M.B., Møller, J. & Tøgersen, F.Aa. (2000). Bayesian contour detection in a time series of ultra-sound images through dynamic deformable template models. *Research Report* **17**, Centre for Mathematical Physics and Stochastics, University of Aarhus.

Hobolth, A. & Jensen, E.B.V. (2000). Modelling stochastic changes in curve shape, with an application to cancer diagnostics. *Adv. Appl. Prob. (SGSA)* **32**, 344-362.

Hobolth, A., Kent, J.T. & Dryden, I.L. (1999). On the relationship between edge and vertex modelling. *Research Report* **7**, Laboratory for Computational Stochastics, University of Aarhus.

Hurn, M.A., Steinsland, I. & Rue, H. (1999). Parameter estimation for a deformable template model. *Preprint Statistics* **5/1999**, Norwegian University of Science and Technology, Trondheim, Norway.

Jensen, E.B.V. (1998). *Local Stereology*. Singapore: World Scientific.

Kent, J.T., Mardia, K.V. & Walder, A.N. (1996). Conditional cyclic Markov random fields. *Adv. Appl. Prob.* **28**, 1-12.

Kent, J.T., Dryden, I.L. & Anderson, C.R. (2000). Using circulant symmetry to model featureless objects. *Biometrika* **87**, 527-544.

Lestrel, P.E. (ed.) (1997). *Fourier Descriptors and their Applications in Biology*. New York: Cambridge University Press.

Loncaric, S. (1998). A survey of shape analysis techniques. *Pattern Recognition* **31**, 983-1001.

Rogers, L.C.G. & Williams, D. (1994). *Diffusions, Markov Processes, and Martingales. Volume 1: Foundations*. 2nd Edition. Chichester: Wiley.

Rue, H. & Hurn, M.A. (1999). Bayesian object recognition. *Biometrika* **86**, 649-660.

Rue, H. & Syversveen, A.R. (1998). Bayesian object recognition with Baddeley's delta loss. *Adv. Appl. Prob.* **30**, 64-84.

Stoyan, D. & Stoyan, H. (1994). *Fractals, Random Shapes and Point Fields. Methods of Geometrical Statistics*. Chichester: Wiley.

Zahn, C.T. & Roskies, R.Z. (1972). Fourier descriptors for plane closed curves. *IEEE Trans. Computers* **C-21**, 269-281.